Blooms of σ^0 in the TOPEX Radar Altimeter Data

GARY T. MITCHUM

College of Marine Science, University of South Florida, St. Petersburg, Florida

DAVID W. HANCOCK III, GEORGE S. HAYNE, AND DOUGLAS C. VANDEMARK

NASA Wallops Flight Facility, Wallops Island, Virginia

(Manuscript received 3 February 2003, in final form 29 January 2004)

ABSTRACT

Data from satellite altimeters are often degraded by the occurrence of unrealistically high radar return cross sections, which indicate a breakdown of the rough surface scattering model used to interpret these measurements in terms of satellite to sea surface height ranges. The TOPEX altimetric data are examined and nearly 200 000 such events during the 7-yr period, 1993–99, inclusive, are identified. The primary purpose of this paper is to make a comprehensive description of where and when these events occur, which is important because many of the communities that make use of the TOPEX data are generally unaware of this phenomenon. It is shown that these events affect almost 6% of the over-ocean TOPEX data, but only approximately 60% of these events are rejected by the recommended TOPEX data flagging. A global description of these events is made, showing that the events are associated with regions of climatologically weak winds (e.g., the summer hemispheres and the western Pacific warm pool region), supporting the existing hypothesis that these events are due to returns from surfaces where centimeter-scale waves are suppressed. The TOPEX results are confirmed with a comparison to anomalous returns from the NASA Scatterometer (NSCAT), and the relationship to very low wind speeds is further examined using the Tropical Ocean Global Atmosphere–Tropical Atmosphere Ocean array (TOGA–TAO) moored buoys. Finally, it is shown that there is some evidence that not all of the events can be accounted for by very low wind speeds. This suggests that future work might exploit the occurrence of these events to study other phenomena, such as surface slicks, that may lead to additional geophysical applications of the altimetric data.

1. Introduction

During the decade since the launch of the TOPEX/Poseidon radar altimetry mission in 1992, satellite altimetric estimates of sea surface height have become a commonly used dataset by many geophysicists, including oceanographers, geodesists, and solid earth physicists. The wide use made of these data is clearly demonstrated in the recent book edited by Fu and Cazenave (2001), for example, and the interested reader is referred to that text for additional information about the applications of satellite altimetry. For our present purposes, however, we simply note that satellite altimeters measure the height of the sea surface by differencing a precise determination of the satellite height, which is derived from independent tracking data, with an estimate of the satellite to sea surface range, which is measured by the radar altimeter. Precise determination of these range values is thus critical to the success of the satellite altimetric method of determining sea surface height variability.

In addition to their range estimates, though, Topography Experiment for Ocean Circulation (TOPEX), which is the National Aeronautics and Space Administration (NASA) altimeter on board the TOPEX/Poseidon satellite, and similar over-ocean satellite-borne radar altimeters also produce estimates of the ocean surface's radar backscattering cross section at normal incidence. This cross section is usually designated by $\sigma^0(0)$, but we will simplify this in the following to σ^0. In this paper we are concerned with possible contamination of altimeter data by what we term "σ^0 blooms," by which we mean regions of over-ocean altimeter data characterized by unusually high σ^0 values. Of course, high backscatter is expected under low wind conditions, so a correspondence of high σ^0 values with low wind speeds is expected. We need to emphasize, however, that these high σ^0 values also signal a breakdown in the basic assumptions used in estimating sea surface height from radar returns, and thus a closer examination of these events has significance beyond the connection to low wind speeds.

Corresponding author address: Dr. Gary T. Mitchum, College of Marine Science, University of South Florida, 140 Seventh Ave. South, St. Petersburg, FL 33701-5016.
E-mail: mitchum@marine.usf.edu

A detailed discussion of the inner workings of the radar altimetry system is beyond the scope of this paper, but we will provide a brief review for the reader unfamiliar with these details. For readers interested in further details, the recent review by Chelton et al. (2001) provides a good starting point. Also, Zieger et al. (1991) have summarized the TOPEX radar altimeter's range tracking and significant wave height estimation using a radar altimeter mean return waveform model. The waveform model development starts from Moore and Williams (1957), who showed that the mean radar power return for incoherent scattering from a rough surface for near-normal-incidence scattering could be expressed as the convolution of 1) the transmitted pulse shape and 2) a term that included effects of antenna pattern, pointing angle, surface properties, and distance. Starting with the convolution model, Brown (1977) used assumptions common to satellite radar altimetry and produced a simplified closed-form expression for the flat-sea impulse response. Later, Rodriguez (1988) pointed out the importance of correcting the Brown flat-surface result to account for the finite radius of the earth, as further discussed in appendix A of Chelton et al. (1989).

All satellite radar altimeters assume the validity of this mean return waveform model, which is in turn based on the assumption of incoherent radar scattering from a rough surface. An example is shown in Fig. 1. The power return estimates under normal conditions are shown as open diamonds, and the fitted waveform model is shown as a solid line. The mean return waveform fit rises to a peak value, which is used to make the σ^0 estimate, and then diminishes (''plateau decay'') at a rate that is a function of the beamwidth and the attitude angle. For any specific beamwidth the fastest possible plateau-relative decay rate occurs for nadir pointing, which has a pure exponential decay after its peak. As the attitude angle is increased from zero, the plateau will decay less rapidly relative to the peak and the decay will no longer be purely exponential. The rate of waveform plateau decay is used to estimate the attitude angle in radar altimeters such as *Seasat*, *Geosat*, and TOPEX. If the waveform estimates in the plateau region decay too rapidly, as is the case during the σ^0 bloom event shown in Fig. 1 (star symbols), most altimetric data processing systems will set an attitude estimation error flag. Since TOPEX has an extremely good attitude control system the true attitude value will never exceed 0.5°, and an estimate greater than this is therefore interpreted as a bad-attitude indicator rather than a meaningful value. That is, the too-rapid plateau decay of Ku-band altimeter waveforms in σ^0 bloom regions is an indication of a partial breakdown of the incoherent scattering model. As the radar altimeter moves into σ^0 bloom regions there is not an easily characterized waveform shape change; we can only report that many, but not all, of the return waveforms in such regions will have the too-rapid plateau decay.

To make our discussion more specific to the TOPEX altimeter, Fig. 2 shows the Ku-band σ^0 values for several data segments during a typical TOPEX 10-day data cycle. The peaks seen in this figure are what we refer to as σ^0 blooms and are characterized by sharp increases of σ^0, on the order of 10 dB, above the surrounding data. Also, most of the apparent blooms exceed 14 dB, which generally indicates invalid data. Of course, most users of altimetry are primarily interested in the final sea surface height estimates. In the summary section below, after we have defined how we selected bloom events, we will present a brief analysis of the effect on the heights. These effects are subtle and will not trouble most users, but do include a small bias error that may affect the most demanding applications of the sea surface height data. The σ^0 blooms persist for several tens of seconds or more, and it is not difficult to identify such blooms in any sufficiently long segment of the TOPEX data. In the figure we also indicate locations where the satellite attitude exceeds 0.6°, which is another indicator of unrealistic data, as discussed above. We have found that excessively high σ^0 estimates in TOPEX bloom regions are invariably accompanied by at least some of the attitude values being flagged. This plot is not atypical, in that there is about a 20% prob-

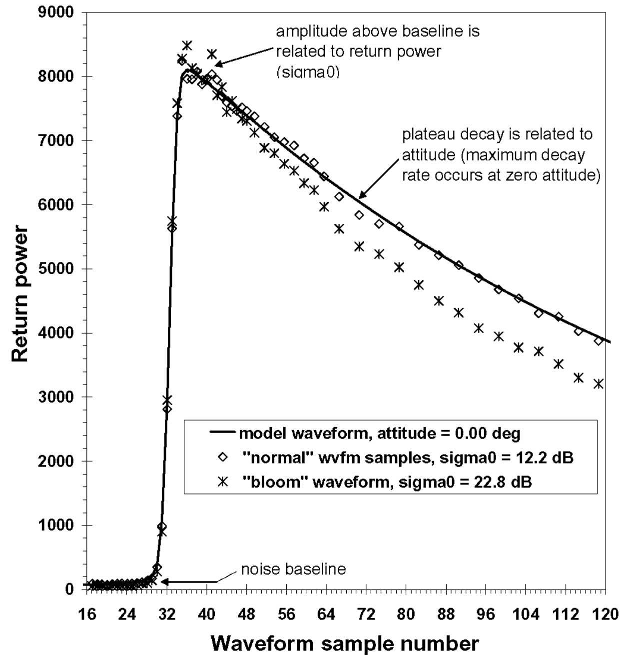

FIG. 1. Illustration of TOPEX Ku-band rescaled waveform observations and model (1-s data averages). The open diamonds show observed power return as a function of waveform sample, which can be considered a time delay. The solid line shows the fit to these samples from the rough surface scattering model discussed in the text. The σ^0 value is proportional to the peak value, while the satellite attitude is proportional to the rate of decay after the time of peak return. The example shown is for a nadir return where the rate of decay is the maximum allowed by the model. The star symbols show the return vs time delay for a sample within a σ^0 bloom region. Note that the fitted σ^0 value is higher and the rate of decay is faster than is theoretically possible from a rough surface.

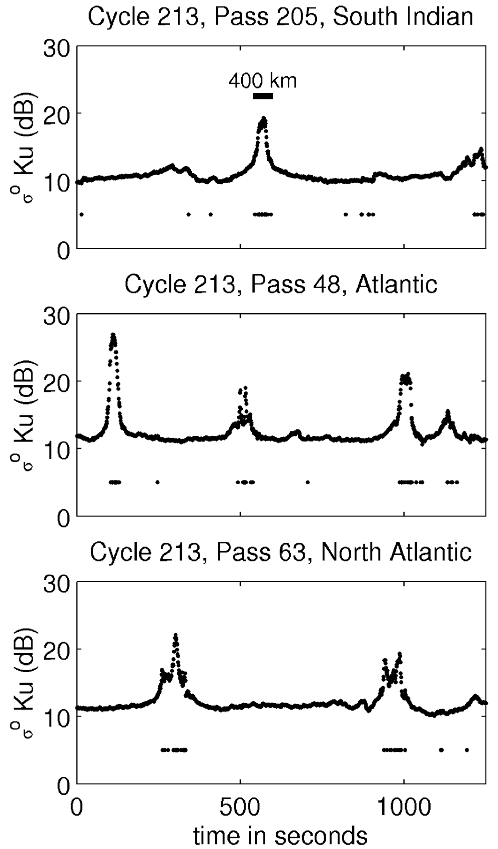

FIG. 2. Representative examples of σ^0 bloom candidates. The σ^0 data from three TOPEX passes during an arbitrarily chosen 10-day data cycle (213) are plotted vs time. (top) To give an idea of the spatial scale, the bloom candidate is shown by the horizontal line to be about 400 km in along-track extent. The dots plotted at a σ^0 value of 5 dB denote 1-Hz samples where the attitude value is greater than 0.6°. Each data segment corresponds to an along-track distance of approximately 8000 km.

ability that at least one σ^0 bloom will be obvious in any 1250-s segment of over-ocean TOPEX data, such as those shown here. That is, as we will detail below, σ^0 blooms exist in more than 5% of all TOPEX over-ocean data.

So what causes the breakdown in the waveform model? An obvious possible cause would be that the sea surface in these regions is not rough, but is reflecting in a specular fashion. This could be due to extremely calm surface conditions, or possibly to the presence of surface slicks that attenuate the short wavelength surface waves that contribute to the surface roughness. This hypothesis has been examined by Garcia (1999), who derived a model for altimeter mean return power from a mostly rough surface containing a few slick or calm areas within the altimeter's footprint. These model predictions were compared with actual altimeter waveforms, but the results were inconclusive. Consequently, at this point we will simply note that very low wind speeds or surface slicks are hypothesized to account for σ^0 blooms. Note also that when we say that the sea surface is not rough, this only means that the centimeter-scale waves are absent, and not that the sea surface is smooth on longer scales. McClain and Strong (1969) showed early on that these types of bloom events could occur even in regions with significant ocean swells, and we also find that many bloom events occur when the significant wave height, which is also measured by the altimeter, is relatively large.

While this paper will focus on TOPEX radar altimeter data, spaceborne radar altimeters have been in use over more than 25 yr and we believe that σ^0 blooms have occurred in all altimeters. We have seen σ^0 blooms in the NASA *Geos-3, Seasat,* and TOPEX altimeters, and in data from the U.S. Navy *Geosat* and *Geosat Follow-On* (*GFO*) altimeters. We have also seen σ^0 blooms in Poseidon altimeter data and, most recently, in data from the new *Jason-1* altimeter. There are σ^0 blooms in data from the *European Remote Sensing Satellite-1* and *-2* (*ERS-1* and *ERS-2*) radar altimeters (R. Francis 2001, personal communication). In short, the σ^0 bloom is a real physical effect and not just an artifact of the hardware details of any single system.

Observations of anomalous behavior from a supposedly smooth sea are not unique to altimeters. It is a common, but often poorly documented, phenomena occurring in various satellite and aircraft remote sensor datasets. In most cases, the geometry of the ocean sensors is such that the smooth surface reflects transmitted energy away from the receiver, causing an extreme loss of signal, or a dark spot. An early report (McClain and Strong 1969) deals with sunglint patterns in high-resolution optical images collected using Application Technology Satellites in the 1960s. Here, optically dark streaks as long as 400 km were observed and attributed to wave suppression under a light wind and stable marine boundary layer conditions. In this paper examples were given of streaks associated with islands, in a large lake, and on a continental shelf where the aspect ratio of the dark regions might be expected to be geometrically constrained. We do not assume that over the open ocean the smooth surface regions will typically form streaks rather than extended areas of enhanced backscatter. Since that time, microwave radars such as the satellite scatterometer and synthetic aperture radar (SAR) have become the most common ocean surface observing sensors, and these dark, smooth surface returns are also observed. SAR imagery, with its high spatial resolution, is often used to study man-made and biogenic slicks on the ocean (Johannessen et al. 2000) as well as other oceanic processes under light wind, smooth surface conditions (Clemente-Colon and Yan 2000). In these cases, large patches of the ocean surface provide little or no surface reflection back to the radar, indicating that centimeter-scale wavelets are absent on the surface. This same process occurs for the radar scatterometer (Carswell et al. 1999; Moller et al. 2000; Plant et al. 1999; Shankaranarayanan and Donelan 2001), but the low-backscatter case is more difficult to document and study because a satellite scatterometer's 25 km × 25 km surface measurement footprint is much larger than for the meter-scale SAR. The scale of these anomalous surface regions is often much less than 25 km, and the scatterometer is therefore usually averaging together smooth and rough surface reflections. Recently, though, Lin et al. (2003) have demonstrated that anomalous backscatter regions observed by the QuikSCAT scatterometer often correspond to regions of high productivity as measured by ocean color. This implies that biogenic slicks are responsible for the unusual backscatter characteristics, and that this spatial smoothing does not preclude observing the blooms. This smearing process must also occur for the altimeter and be dependent upon the spatial extent of smooth and rough regions within the altimeter's 8 km × 14 km footprint. As mentioned above, the phenomena should be evident in any satellite sensor that is able to discern surface roughness at the centimeter scale. One recent example is the near-nadir-viewing Ku-band rain radar aboard the Tropical Rain Measurement Mission (TRMM) satellite. This system obtains anomalously large σ^0 values for ocean surface reflections at a rate that is similar to that obtained with the altimeters (R. Meneghini 2002, personal communication).

Of course, most altimeter data users have no interest in σ^0 itself, although they may be interested in the estimates of ocean wind speed that can be obtained from a semiempirical (inverse) relationship between σ^0 and wind speed (Chelton et al. 2001). A σ^0 bloom will cause an already low wind estimate to become even closer to zero, but by an amount that is of no practical significance to the wind speed data user. Most of the altimeter data in σ^0 bloom regions will have sufficiently odd waveform shapes that some of the data flags will be set; but we are concerned that the recommended editing criteria (e.g., Benada 1997; Callahan 1993) will not remove all of the bloom-contaminated data. In general, as we will document below, altimeter data users fortunately remove most of the bloom-contaminated altimetry data by using suggested editing criteria, and are not aware of the bloom phenomenon. An exception is a recent paper by Quartly et al. (2001), which discusses various altimeter artifacts and properties of radar altimeter ocean waveforms. Figure 2 in that paper notes strong positive anomalies in σ^0 in the fourth and fifth ensembles in the plot, and we believe that positive anomaly to be another σ^0 bloom example.

In addition to our interest in correct data flagging for σ^0 blooms, we have long wondered if the spatial and temporal distribution of the blooms had any interesting geophysical correlates. That is, could the bloom distribution be a signal of practical importance in itself and not just a bothersome artifact in altimeter data? We want to explore that question in the future, but our intention here is to first make a comprehensive description of where and when σ^0 blooms occur in the TOPEX data, which has not been done previously. We will evaluate the possibility that low wind speeds can account for the majority of the bloom occurrences, and we will also make estimates of how successful the usual editing is at eliminating data that is likely contaminated by σ^0 blooms.

2. Space–time distribution of TOPEX blooms

In order to address the space–time distribution of σ^0 blooms it is necessary to first decide on an automatic method for identifying blooms since we are dealing with 7 yr (1993–99) of 1-Hz data. Some of the challenges inherent in creating the desired database are demonstrated in Fig. 2. The event seen in the top panel is a fairly obvious case, as is the first one in the middle panel. On the other hand, the second event near t = 500 s in the middle panel and the event near t = 950 s, could easily be classified as a single fairly broad event, or as two separate, but closely spaced, events. Another problem is setting thresholds. For example, is the event in the middle panel near t = 1150 s, an event or not? After looking into this problem for some time we came to mistrust criteria based simply on the maximum σ^0 values, and instead developed a more complex, but we believe more reliable, algorithm. Also, because of the large data volume we decided to focus on the Ku band in order to keep the calculations and analyses reasonably tractable, at least until we could determine how frequent these events actually were. It would certainly be interesting and useful to also examine blooms in the C-band data, but we decided to look first at the Ku band because of its central role in the estimation of the sea surface heights. We do, however, note that a joint analysis of the Ku- and C-band blooms would be a very useful topic for future work. For example, examining both bands simultaneously might allow a better determination of the effect of rain in creating smooth sea surfaces that might cause bloom events (G. Quartly 2003, personal communication).

As discussed above, σ^0 blooms are often associated with invalid satellite attitude values, and this is generally one of the clearest indicators of a σ^0 bloom event. Again, this is because the large attitude values are not real, but are effectively a flag indicating a breakdown in the waveform model. We therefore do not simply set a threshold based on σ^0 alone, but we also require invalid attitude values during at least a portion of the bloom event. As seen in Fig. 2, these invalid attitude values are generally associated with the bloom events, but do not occur throughout the event. Nevertheless, the occurrence of these invalid attitude values is a clear indicator of a σ^0 bloom event. It is tempting to attempt to identify events based on assumptions of how the waveform shapes might evolve as the altimeter's footprint begins to encounter a bloom region, passes through it, and then moves out of it. We in fact examined a large number of waveforms for a specific signature, but we could not identify anything useful. As we noted in the introduction, all we can really say is that most, but not all, of the waveforms have unusual attitude values during a bloom event.

After some study of the TOPEX data, we settled on a two-step procedure for identifying σ^0 blooms. In the first pass through the data, we identified all points where the TOPEX data are taken in deep water, where the Ku-band altimeter is in fine-track mode, where the Ku-band σ^0 value is greater than 14.0 dB, and where the waveform-estimated attitude value is greater than 0.30°. Following this initial identification of potential bloom events, a second pass was made to create the final bloom dataset. This second pass is necessary because in a typical bloom there will be regions in which the attitude values are reasonable. As seen in Fig. 2, the high attitude values will turn on and off through a region of high σ^0. Our examination of the TOPEX data indicates that it is reasonable to expect a coherence interval of 10 s or so in passing through a bloom region. That is, if there is a bloom candidate at time T (where the bloom candidate is selected in the first pass through the data) and another bloom candidate at time $T + 4$ s, these probably are not two separate blooms but two different signals from a single bloom. In this second pass, then, this requirement of a minimum coherence length allows bloom regions such as the one seen in the middle panel of Fig. 2 near $t = 500$ s to be assigned to one or two events depending on the temporal separation. Bloom candidates of shorter duration than 10 s are not accepted, and in much of the following we only report results from bloom events where the durations exceed 20 or 25 s. This undoubtedly causes us to miss some bloom events, but we decided to be conservative in this respect in order to not overstate the importance of these events to the data editing issue. That is, we restrict our attention to events that we are nearly certain are true bloom events, and that we would hope the data editing would identify.

For each bloom event identified, several parameters were recorded. First, the maximum σ^0 value was saved, as was the duration of the event. In addition, the exact time and geographic location was noted, in addition to a variety of other parameters that will not be used in this first description of the bloom events. During the 7 yr of TOPEX data that we examined, we identified a total of 189 097 bloom events with the above (conservative) procedure. If we add the durations of these events, we have a total of 91.4 days of data affected in 7 yr. When we consider that the TOPEX altimeter is on approximately 90% of the time (the French Poseidon altimeter is on during the remainder of the time), this means that the altimeter is in a σ^0 bloom event approximately 4.0% of the time. If we only consider times when the altimeter is over the deep ocean, this rises to approximately 5.7% of the time. Clearly, these events are not rare at all.

These numbers allow us to also make a gross estimate of how effective the usual data editing procedures are

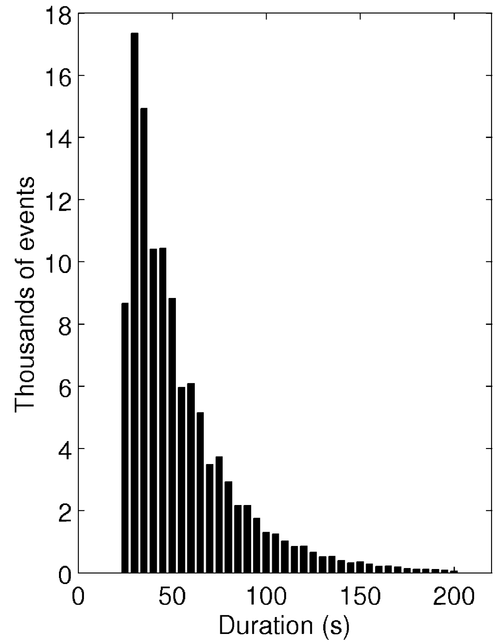

FIG. 3. Distribution of bloom events vs temporal duration. Only σ^0 bloom events of duration longer than 25 s are used. A small number of events longer than 200 s in duration are also suppressed.

at eliminating data that are clearly under σ^0 bloom conditions. To address this point, we first restrict our attention to events of more than 25-s duration, which is where we have confidence that these are real σ^0 bloom events. Of the 189 097 events identified, 114 416 met this criterion, and these events spanned a total of 5 905 703 s, or about 68 days. If the normal editing criteria are applied when processing the TOPEX data, the total duration of data affected by bloom events drops to 2 577 172 s, or about 30 days, meaning that the normal editing removes approximately 56% of the affected data records. Note, however, that because our definition of bloom events is intentionally conservative, this should probably be considered an optimistic estimate. We also considered whether adding an editing criterion that rejected data when the satellite attitude exceeded 0.6° would substantially improve the situation. Normally the data are only flagged when the attitude is flagged as invalid. We found that including this additional editing criterion only flags an additional 155 983 s (about 2 days) of the suspect data, leaving 41% of the bloom events unflagged.

The distributions of the blooms events in terms of the durations and magnitudes are shown in histogram form in Figs. 3 and 4, respectively. For the durations we show events greater than 25 s in duration (62% of the total number of events satisfy this criterion). Recall also that these events all have σ^0 values exceeding 14 dB. Of these events, 25% exceed 50.2 s, 50% exceed 30.8 s, and 75% exceed 21.1 s. For the magnitudes, 25% exceed 23.0 dB, 50% exceed 15.5 dB, 75% exceed 14.2 dB,

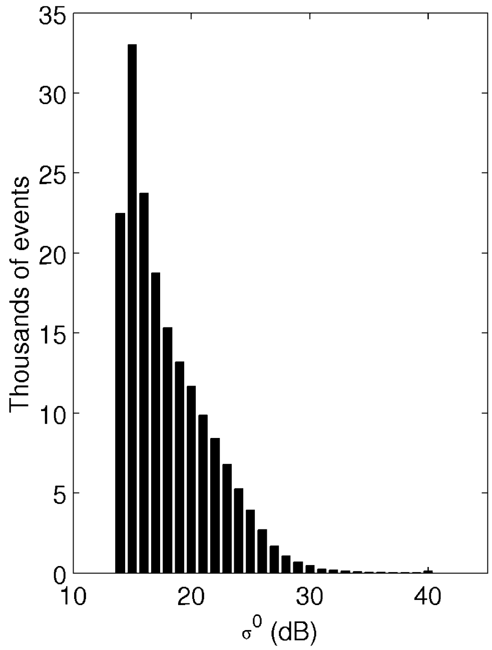

FIG. 4. Distribution of bloom events vs the maximum σ^0 value within the bloom. Only bloom events of duration greater than 25 s and magnitude greater than 14.5 dB are used. The small increase at 40 dB represents the few events associated with sea ice in the Sea of Okhotsk.

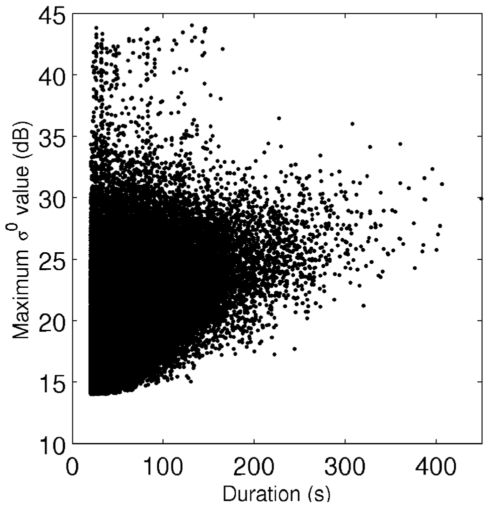

FIG. 5. Scatterplot of maximum σ^0 value and duration for the bloom events identified in this study. Note the set of relatively short-duration events with σ^0 values greater than 35 dB. These are associated with sea ice in the Sea of Okhotsk.

and 25% fall between 14.2 and 14 dB, which was the cutoff magnitude used to define a possible event. Figure 5 shows the relationship between duration and magnitude, which reveals an interesting anomaly. There is a fairly large number of events with large magnitudes but durations shorter than 150 s that do not fit with the overall distribution. When the locations and times associated with the events that exceed 35 dB are plotted (not shown), we find that these events all occur in the Sea of Okhotsk in the Northern Hemisphere winter. We believe that these events are due to occurrences of sea ice (which can create specular-type returns) that are not flagged in the TOPEX database. Since these events are geographically very constrained, and the total number of events is small, we will not consider events of this magnitude any further, but we do note that the ice flagging for TOPEX might be improved.

In order to examine the space–time distribution of the bloom events we next examined the spatial distributions of the events on a month-by-month basis. An example is shown in Fig. 6, which contrasts conditions in the Northern Hemisphere winter (top panel) and summer (bottom panel). In this figure we see an indication of a relationship to wind speed, with the summer hemisphere containing the majority of the events, especially in the Northern Hemisphere summer. For example, the location of the intertropical convergence zone (ITCZ), where light winds are expected and thus more σ^0 blooms might be expected, is seen in all three basins in the August map. Also, the winter/summer contrast is more apparent in the Northern Hemisphere, which is consistent with a larger seasonal variation in the wind speed in the Northern Hemisphere.

By considering all such monthly distributions together, we can show the spatial distribution of σ^0 blooms (Fig. 7, top panel), as well as the temporal modulations (Fig. 7, bottom panel). In the spatial distribution we see that the western Pacific warm pool area, which is a region of climatologically light winds, is also an area

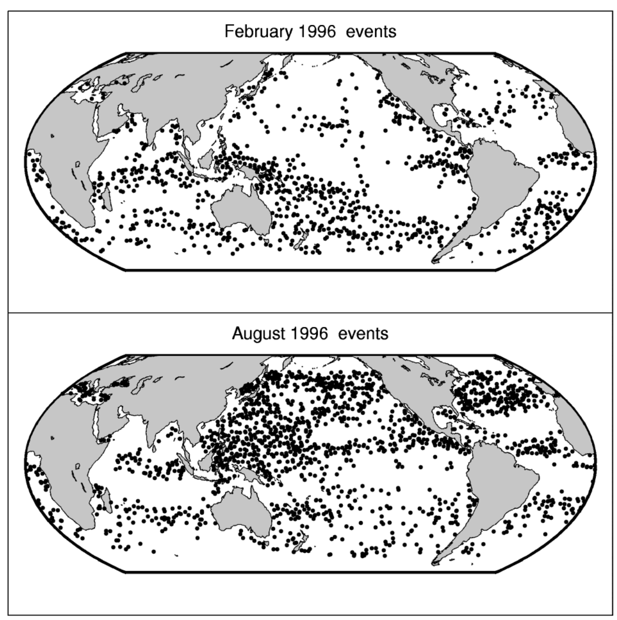

FIG. 6. Locations where bloom events are observed (top) in Feb 1996 and (bottom) in Aug 1996. The contrast between the two is typical of other years and reflects the difference between the summer and winter hemispheres.

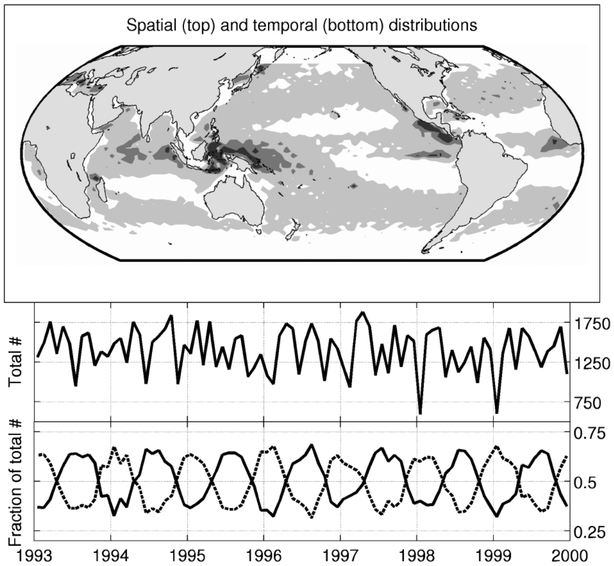

FIG. 7. Spatial and temporal distributions of all events observed. Only events of duration greater than 25 s are included in this analysis. (top) The spatial distribution is shown. To make this plot, the number of events was counted in 2° lat by 4° lon bins. The three shades of gray (from light to dark) correspond to 25–75, 75–125, and more than 125 events, respectively. (middle) The number of events vs time obtained by summing the number of events in daily bins. (bottom) The time series of the fraction of the total number of events within each daily bin that occurs in the Northern Hemisphere (solid) and the Southern Hemisphere (dashed). Note the clear seasonality in the (bottom), indicating that events occur preferentially in the summer hemisphere.

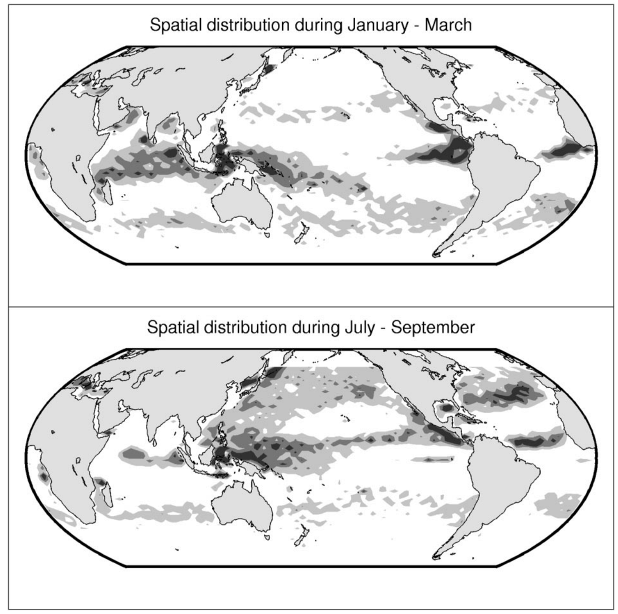

FIG. 8. Spatial distributions during (top) the Northern Hemisphere winter and (bottom) summer. Winter is defined as the 3-month period Jan–Mar, inclusive, and summer is defined as Jul–Sep, inclusive. Of course, these periods could equally well be described as Southern Hemisphere summer and winter, respectively. The events were counted in 2° lat by 4° lon bins, and the three shades of gray (from light to dark) correspond to 10–20, 20–30, and more than 30 events, respectively.

where a large number of σ^0 blooms occur. Large numbers of events are also seen in the eastern Pacific cold tongue region and along the western coasts of Central America and equatorial West Africa. We also see a dearth of events in the trade wind belts in all basins, as well as small numbers of events at the highest latitudes observed. The temporal structure (bottom panel) is even more suggestive of a relationship to wind speed. Although the total number of events is difficult to interpret, when the events are plotted as the fraction occurring in the Northern versus Southern Hemisphere, there is an extremely clear annual variation, with a clear preference for the σ^0 blooms to occur in the summer hemisphere.

This preference for the summer hemisphere can also be seen by plotting the spatial distribution of the bloom events during January–March and during July–September (Fig. 8). The top panel, which is the Northern Hemisphere winter, shows an almost complete lack of events in the Northern Hemisphere, in complete contrast to the bottom panel, which is during the Northern Hemisphere summer. This interhemispheric difference is superimposed on the events associated with the western Pacific warm pool and the ITCZ noted above, but is still extremely clear, indicating again a likely relationship to wind speed. As another check on the temporal modulations associated with the bloom events, we also stratified the data into events occurring during the El Niño event of 1997/98, and the La Niña event immediately following (Fig. 9). Focusing on the equatorial Pacific, we see that during the El Niño event, when the trade winds have weakened, there are many more bloom events in the central equatorial Pacific. In contrast, during the La Niña, there are more events in the warm pool and cold tongue regions, which is consistent with strengthened trade winds in the central Pacific and weakened winds in these regions.

It is natural to ask whether these descriptions in terms of histograms and space–time distributions change significantly depending on the magnitudes or durations of the events. We evaluated this question by looking into the temporal and spatial distributions of the largest and smallest thirds of the events in terms of both duration and magnitude. Figure 10 shows the results for the spatial distributions. The four subsets show similar spatial patterns, although the pattern is slightly more pronounced for the largest events, which is not surprising since these are the events that are the most reliably determined. But the similarity of pattern for the smallest events indicates that even for the borderline events, we are still most likely capturing real events. The temporal pattern (not shown) for all the subsets clearly indicates the same out of phase relationship between the hemispheres that is seen in Fig. 7.

We also investigated the distribution of the bloom events as a function of the time of day (Fig. 11). In this

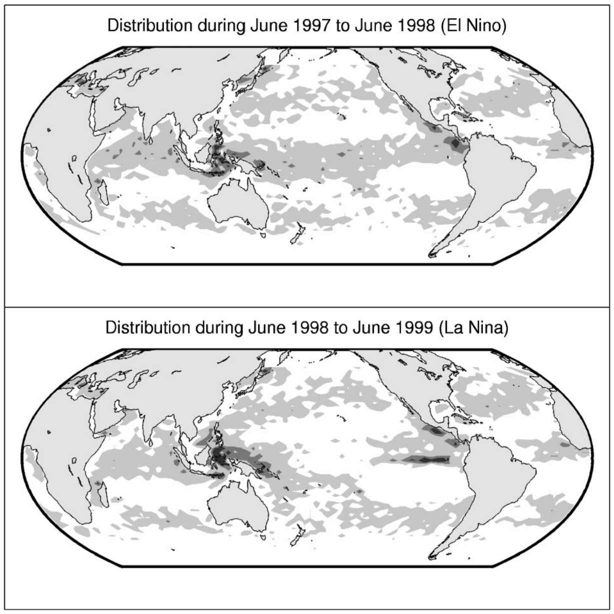

FIG. 9. Spatial distribution of events during (top) El Niño conditions and (bottom) La Niña conditions. The large El Niño and La Niña events of 1997/98 and 1998/99, respectively, are used to examine interannual changes in the occurrence of the bloom events. The events are counted in 2° lat by 4° lon bins, and the three shades of gray (from light to dark) correspond to 5–15, 15–25, and more than 25 events, respectively. Note in particular the changes in the tropical Pacific Ocean.

case only blooms that exceed 25-s duration and have a maximum σ^0 greater than 14.5 dB were used, which leaves 112 323 events. The events were then simply counted according to the local hour of the day. There is a large background, which means that the local time of the day is not a strong predictor for a bloom event. We also see, however, a clear modulation on top of this background that depends on the time of day. There is a subtle day/night difference, but the most striking features are the distinct minima just after local sunrise and sunset. We speculate that this modulation is further evidence that the bloom events are associated with light winds, although we cannot document that here. We point out, however, that if the blooms tend to occur in regions where the winds tend to be light, then the wind state at any given location (i.e., whether it is simply light or whether it has nearly vanished) should depend mainly on the surface heat balance and the attendant forcing of the atmospheric boundary layer. At these times of day the heating is transitioning between daytime conditions dominated by insolation and nighttime conditions dominated by outgoing longwave radiation. Previous work (e.g., Wu 1991; Vandemark et al. 1997) has documented the effect of atmospheric stability on microwave measurements, and we suggest that these are the times of the day when atmospheric stability might most likely be anomalous.

To summarize, the basic spatial and temporal distribution of the σ^0 blooms have been described, and we find that the blooms are much more likely to occur in

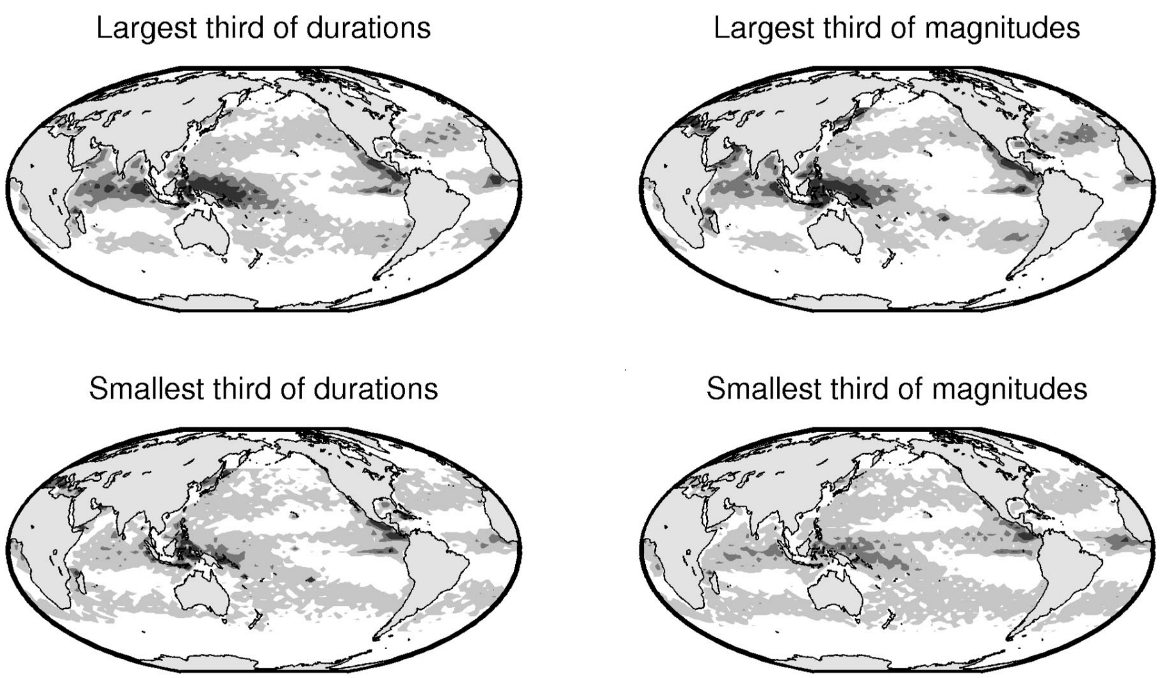

FIG. 10. Comparison of the spatial distributions for the events with the smallest and largest durations and σ^0 magnitudes. For each plot the total number of events were separated into thirds based on (left) the durations or (right) maximum σ^0 values. The number of events in the largest and smallest thirds subsets are then contoured. The number of events is counted in 2° lat by 4° lon bins, and the three levels of gray (from light to dark) on each plot correspond to 10–25, 25–40, and more than 40 events, respectively.

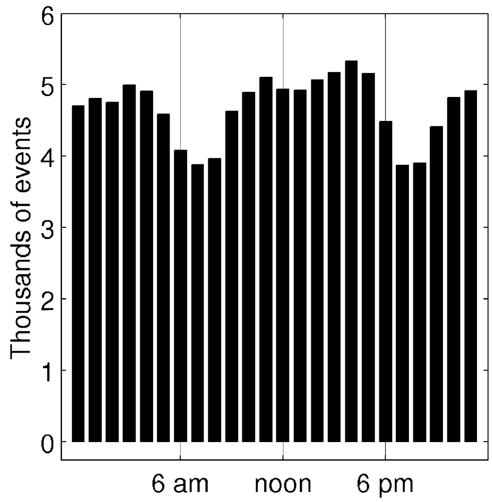

FIG. 11. Distribution of events vs local hour of the day. For each event the central time is converted to the local hour of the day based on the Greenwich time and the longitude where the event occurred. Since the events are typically less than 200 s in duration, using the central time is acceptable. The vertical grid lines on the plot indicate 0600, 1200, and 1800 local time. Only events of duration longer than 25 s and with maximum σ^0 value greater than 14.5 dB are used in this analysis. Note the distinct shortage of events just after dawn and dusk, meaning just after 0600 and 1800 LT.

the summer hemisphere, and in regions where climatologically we expect light winds. Also, this indication of a relationship to wind speed, which is not unexpected, is not sensitive to our definition of a bloom, in the sense that the events with the largest and smallest σ^0 values and with the longest and shortest durations have similar distributions. In the following section we will more closely examine the suggested relationship of the bloom events to low wind speeds. As noted in the introduction, we are also interested in bloom events that are not associated with low wind speeds, so a closer examination of the gross relationship between bloom events and low wind speeds detailed in this section is of particular interest.

3. Relationship to wind speed

In the previous section we have given a global description of where and when the σ^0 blooms occur, and we have pointed out that, as expected, the occurrence of bloom events coincides with regions and times where weak winds should occur. To this point, however, since we were intending to give a description of the bloom statistics rather than attribute causes, the relationship to wind has only been in a climatological sense. In this section we will examine collocations of the bloom events with global data from the NASA scatterometer (NSCAT) and with tropical Pacific wind observations from the Tropical Ocean Global Atmosphere–Tropical Atmosphere Ocean array (TOGA–TAO) buoys. The purpose here is twofold. First, we want to demonstrate more conclusively that the hypothesis that these events are associated with weak winds is reasonable. And second, we are interested in whether there is any evidence that significant numbers of bloom events occur when the winds are not likely to be weak. If this occurs very often, then additional causes, such as surface slicks, must be examined more closely. Also, there is then the additional possibility of other geophysically interesting causes that the blooms might be used to study.

For the comparison with the NSCAT wind data, we used the database described by Gourrion et al. (2002), which defines a collocation between the NSCAT and TOPEX observations when there is an NSCAT measurement within 12 km of the TOPEX ground track where a bloom event occurs and within 1 h before or after the TOPEX pass. When the bloom occurrences are binned according to the NSCAT-inferred wind speeds (Fig. 12), we see that nearly all of the σ^0 blooms events are associated with winds that are less than 3 m s^{-1}. We show the binning for several different incidence angles, and this does not significantly affect the conclusion. Basically, when the TOPEX altimeter sees a bloom event, the probability is extremely high that the scatterometer will infer very light winds. We do not, however, interpret this result as confirming the hypothesis that the bloom events are simply associated with light winds. This is because the scatterometer does not measure wind speed directly, but instead measures the surface roughness due to short capillary–gravity waves in the same fashion as the altimeter. The scatterometer, however, views the surface at an angle, meaning that a very smooth surface returns little power, leading to the light wind speed inference. For the scatterometer, wind speeds less than 3 m s^{-1} basically mean that the instrument is seeing an essentially smooth surface, which in the case of the altimeter would lead to a σ^0 bloom. We therefore conclude from this comparison with the scatterometer data that both instruments are consistently inferring a surface with few short waves, which confirms that the bloom events identified in the TOPEX data are real, and not an artifact of our selection criteria.

In order to assess the relationship with wind speed more directly, in situ measurements are required, although such measurements that are coincident with TOPEX are difficult to obtain. There are, however, a large number of buoys measuring wind speed, along with other parameters, in the tropical Pacific. This array of buoys is referred to as the TOGA–TAO network, which grew out of the TOGA-observing system. The interested reader should see McPhaden et al. (1998) for a complete discussion of the TOGA-observing system, including the TAO buoys. We used the data from 70 TAO buoys, although not all of these were near a TOPEX track and not all cover the entire time period we are considering. Even with 70 buoys, the probability of having buoy data very near the TOPEX track and having a σ^0 bloom occur at that location is rather small. Note also that this prob-

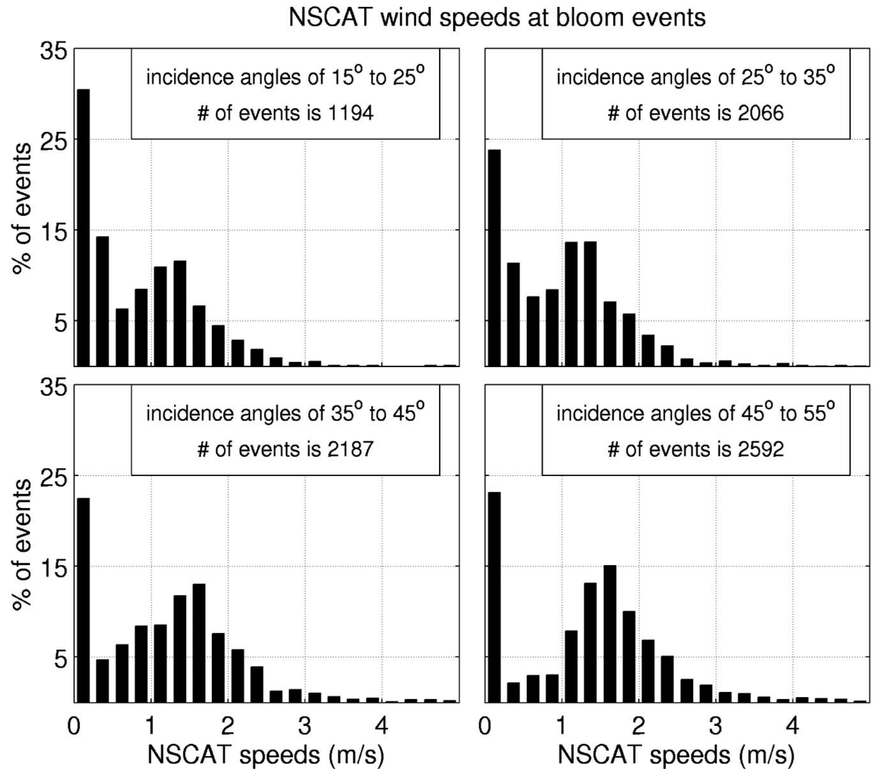

FIG. 12. Comparison of coincident NSCAT wind observations to TOPEX σ^0 bloom events. Coincident events were defined as when NSCAT made a wind observation within 12 km spatially and within 1 h temporally of the bloom event. The wind observations are shown for four different NSCAT incidence angles (see inset on each panel of the plot). Typically 1000 to 2000 events are captured at each incidence angle (see inset for exact number). Within each panel, the distribution of wind speed during the bloom events is given, and it is seen that the NSCAT-inferred wind speeds are typically light.

ability depends critically on what is considered to be a near-enough collocation to be useful.

We will first restrict our attention to only the most significant σ^0 bloom events, which are defined as having durations greater than 100 s and a maximum σ^0 greater than 20 dB, and we will also require that the bloom is located less than 20 km from a TAO mooring. When doing this first comparison we took the wind speed estimate from the buoy to be a single spot sample from an hourly time series. There are eight σ^0 bloom events that satisfy these criteria. For these eight events, the maximum wind speed observed at the TAO mooring was 2.9 m s^{-1}, with the median wind speed being only 1.3 m s^{-1}, which supports the light wind hypothesis since the typical wind speeds observed at the buoys were 6–7 m s^{-1}.

Because the buoy is not directly under the TOPEX track, however, this is not obviously the best choice. It is very possible that the light wind speeds are of small scale spatially and of short duration temporally. Since we are also interested in determining if there is any evidence of significant blooms occurring when the winds are not light, we wanted to make another estimate of wind speed that would estimate the lightest winds that *might* have been associated with the event. To make this estimate, we determined the minimum wind speed that occurred at the buoy during a 48-h (full width) window centered on the σ^0 bloom event. For the eight events just discussed, when this method is used to make the collocated wind speed estimate, the maximum and median wind estimates drop to 1.1 and 0.6 m s^{-1}, respectively, which supports the idea that all of the events are associated with light winds.

Of course, eight events is an extremely small sample of the total number of bloom events that we found. We therefore decided to allow the distance from the buoy to the TOPEX σ^0 bloom event to be as a large as 100 km. With this definition, we have 545 bloom events with collocated wind observations. We used both spot samples to estimate the wind speed as well as the estimate equal to the minimum wind speed in a 48-h window surrounding the bloom event. The results of this comparison are shown in Fig. 13. In the left-hand panels the spot samples for wind speed are used, while the 48-h minimum estimates are used in the right-hand panels. The top panels show the distribution of the 545 bloom events as a function of the wind speed estimates. The bottom panels show the distribution of all of the

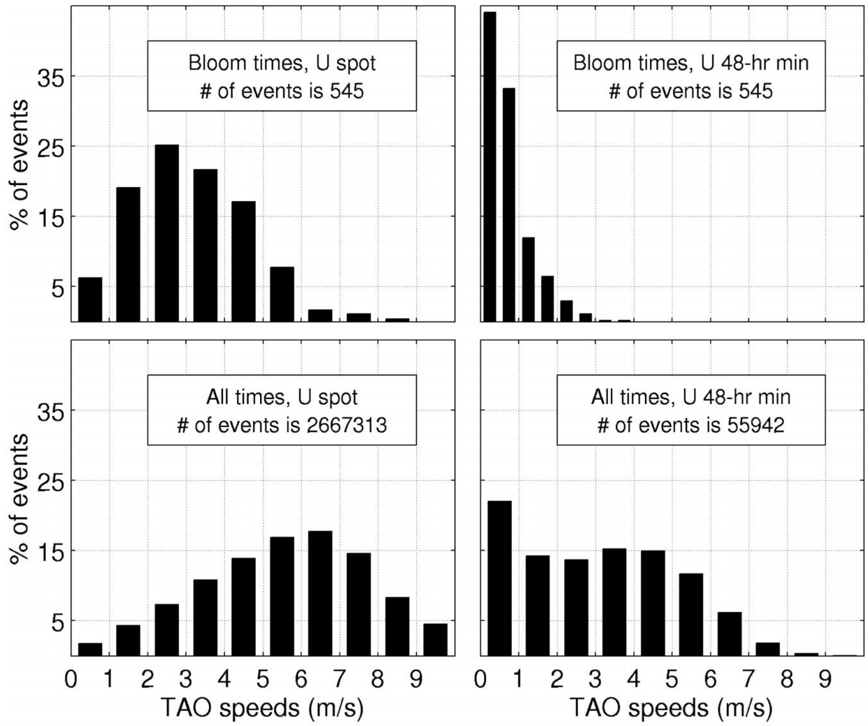

FIG. 13. Comparison of coincident TOGA–TAO wind observations to TOPEX σ^0 bloom events. For this comparison coincident observations were defined as being within 100 km of the TOPEX bloom event. Temporal coincidence is nearly exact since the TOGA–TAO observations are hourly. (top) The distribution of TOGA–TAO winds during the blooms events are shown. (bottom) For comparison, the distribution of the TOGA–TAO events at all times is shown, which can be used to assess the degree to which the winds during the bloom events are anomalously light. (left and right) Two different definitions of the appropriate TOGA–TAO wind speed to use. (left) The closest hourly wind sample is used. (right) The minimum wind speed in a 48-h interval centered on the time of the bloom event is used.

wind estimates regardless of whether or not a bloom is present. Comparison of the top and bottom panels thus allows a determination as to whether the winds are anomalously weak during the σ^0 bloom events.

Considering the spot samples for the wind speed first, the wind speed during bloom events (top-left panel) is less than 5 m s^{-1} in most of the cases. For the wind estimates as a whole, however, (bottom-left panel) the typical wind speed is typically 6–7 m s^{-1}, and it is clear that these two distributions are quite different. That is, the bloom events are generally associated with winds that are at the lower end of the overall distribution. The comparison with the 48-h minimum estimate of the wind speed is similar, in that the nearly all of the bloom events are associated with speeds less than 2 m s^{-1}, whereas estimates this small only occur about one-third of the time in the buoy record as a whole.

These comparisons using the TAO buoy winds certainly support the idea that the σ^0 bloom events are generally associated with anomalously low wind speeds. But we also note from Fig. 13 that approximately 10% of the events are associated with spot-sampled winds greater than 5 m s^{-1}. Even when the 48-h minimum wind speed is used, approximately 5% of the blooms are still associated with speed estimates greater than 2 m s^{-1}. Given that we had to allow separations up to 100 km between the TOPEX track and the buoy location to make these comparisons, it is difficult to conclude very much from this, but we consider this observation suggestive of other causes for σ^0 bloom events beyond still wind conditions.

4. Summary

Our primary purpose here has been to make a description of the events we have termed σ^0 blooms in the TOPEX dataset, although our long-term interest is to determine whether the occurrence of these events can be exploited for additional applications of radar altimetric data. Such a description is an important first step to this goal, and it is also important for the majority of TOPEX data users that are not familiar with this potential problem with the TOPEX data. These events are not unique to TOPEX, but affect all satellite altimeters, and other types of data as well. For example, we have shown that the events observed in the TOPEX data are also seen in the NSCAT scatterometer data when the

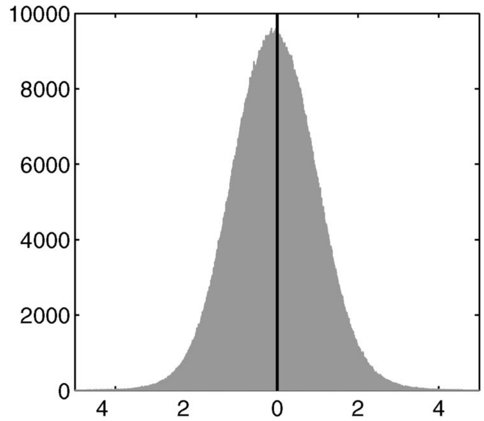

FIG. 14. Histogram of normalized sea surface heights during bloom events. The method of computation is described in the text. The mean and std dev of the distribution are −0.06 and 1.03, respectively. The vertical solid line is at zero deviation.

two instruments measure the same area of the sea surface.

As we mentioned in the introduction, we understand that most users of altimetry data are primarily concerned with the effect the blooms might have on the final sea surface height estimates. In order to roughly quantify the effect on sea surface height we did the following calculation. First, for every bloom event that we identified we extracted all of the sea surface height estimates that were not removed by the normal data flagging procedures. We found just over 3 million such height estimates from the nearly 200 000 bloom events. For each one we computed a normalized height deviation by subtracting the mean of the time series at the spatial location of the height estimate and dividing by the standard deviation of the time series. In principle, then, if the blooms have no effect on the height data, these deviations should be normally distributed with zero mean and unit standard deviation. Variations from this indicate an error associated with the bloom events. As a check we also randomly selected a point from the time series at each point. These randomly selected data were indeed normally distributed with zero mean and unit standard deviation, as expected. The histogram of the normalized height data during bloom events (Fig. 14) shows nearly the same result, but close examination shows a slight shift to negative values. The mean of the distribution is −0.06, whereas the standard error of the mean (computed by assuming that there is only one degree of freedom per bloom event) is less than 0.003. This negative bias, while small, is thus highly significant in a statistical sense. Further, there are nearly 4 times as many points in the negative tails of the distribution than on the pos-

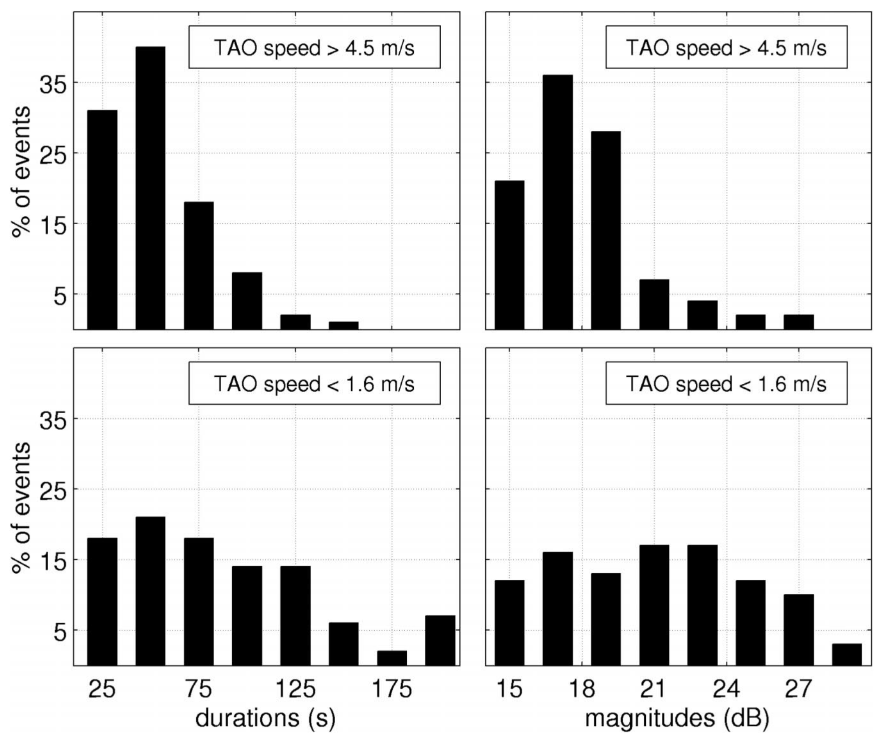

FIG. 15. Bloom characteristics when TOGA–TAO winds are relatively large or relatively light. For the 545 coincident events described in Fig. 13, (left) the bloom durations and (right) the maximum σ^0 values are shown for winds (top) >4.5 and (bottom) <1.6 m s^{-1}. Note that when the winds do not appear to be light during a bloom event (top), the distributions indicate that the blooms events are substantially shorter and of lesser magnitude.

itive side. Given that the typical standard deviation for the TOPEX time series is 100 mm, this bias error is on the order of 6 mm. This is small enough that most users will not be affected, but we also note that this is not very much less than the random error estimates (order of 20 mm) for TOPEX heights made from comparisons to tide gauges (Mitchum 2000), which suggests caution for users making the most demanding applications of the sea surface heights.

The method we have developed to identify bloom events is intentionally conservative, yet we still find that nearly 6% of the over-ocean TOPEX data are affected. And about 40% of these events are not removed by the recommended TOPEX data flagging, which suggests that improvements to the data flagging might be possible. We have found that most of the events are clearly associated with geographic regions where we expect the winds to be very light, as in the summer hemispheres of the oceans and along the intertropical convergence zones in all oceans, for example. We also document a change during ENSO events that is consistent with the wind changes associated with these events. This relationship to low wind speeds is further confirmed via an analysis of events occurring near the TOGA–TAO ocean buoys. Hence, it appears that the usual explanation for these events, a lack of centimeter-scale ocean ripples due to low wind speeds, can account for the majority of the events we observe.

In conclusion, however, we would like to return to our interest in σ^0 bloom events that might be associated with geophysical conditions other than low wind speeds. Recall that we suggested in the previous section that some of the bloom events might not be associated with low wind speeds. To further evaluate this possibility, we have looked at the distributions of the bloom durations and magnitudes for small (<1.6 m s^{-1}) and large (>4.5 m s^{-1}) wind speeds (Fig. 15). The spot-sampled wind speed estimates are used in this case. For the low wind speeds, the durations and magnitudes are fairly featureless. When the wind speeds are large, however, there is a clear tendency for the bloom events to be of shorter duration and of smaller magnitude. It is possible that this indicates problems with how we identified the bloom events, but the scatterometer comparison shown earlier argues against that interpretation. It is also possible that these smaller events are also smaller in scale spatially, and the wind at the buoys is simply not reliable. This possibility is impossible to discount. There is another possibility, however, which is that low wind speed does not account for all of the σ^0 bloom events, and that the events of other origin tend to be of somewhat smaller magnitude and of shorter duration than typical σ^0 bloom. We cannot address that further possibility at present, but we would suggest it as an interesting area for future work.

Acknowledgments. This research was supported by NASA as part of the *Jason-1* project at the Jet Propulsion Laboratory under Contract NAG5-5202. We thank G. Quartly and A. Busalacchi for helpful comments and discussions.

REFERENCES

Benada, R., 1997: PODAAC merged GDR (TOPEX/POSEIDON) generation B user's handbook version 2.0. Jet Propulsion Laboratory Doc. JPL D-11007, 131 pp.

Brown, G. S., 1977: The average impulse response of a rough surface and its applications. *IEEE Trans. Antennas Propag.,* **AP-25,** 67–74.

Callahan, P. S., 1993: TOPEX GDR user's handbook. Jet Propulsion Laboratory Doc. JPL D-8944 Rev. A, 84 pp.

Carswell, J. R., W. J. Donnelly, R. E. McIntosh, M. A. Donelan, and D. C. Vandemark, 1999: Analysis of C and Ku band ocean backscatter measurements under low-wind conditions. *J. Geophys. Res.,* **104,** 20 687–20 701.

Chelton, D. B., E. J. Walsh, and J. L. MacArthur, 1989: Pulse compression and sea level tracking in satellite altimetry. *J. Atmos. Oceanic Technol.,* **6,** 405–438.

——, J. C. Ries, B. J. Haines, L.-L. Fu, and P. S. Callahan, 2001: Satellite altimetry. *Satellite Altimetry and Earth Sciences,* L.-L. Fu and A. Cazenave, Eds., Academic Press, 1–131.

Clemente-Colon, P., and X. H. Yan, 2000: Low-backscatter ocean features in synthetic aperture radar imagery. *Johns Hopkins APL Tech. Dig.,* **21,** 116–121.

Fu, L.-L., and A. Cazenave, Eds., 2001: *Satellite Altimetry and Earth Sciences: A Handbook of Techniques and Applications.* Academic Press, 463 pp.

Garcia, A., 1999: Study of the origins of the σ^0 blooms. M.S. thesis, Dept. of Electrical and Computer Engineering, Virginia Polytechnic Institute and State University, Blacksburg, VA, 159 pp.

Gourrion, J., D. Vandemark, S. Bailey, B. Chapron, G. Gommenginger, P. Challenor, and M. Srokosz, 2002: A two-parameter wind speed algorithm for Ku-band altimeters. *J. Atmos. Oceanic Technol.,* **19,** 2030–2048.

Johannessen, O. M., S. Sandven, A. D. Jenkins, D. Durand, L. H. Pettersson, H. Espedal, G. Evensen, and T. Hamre, 2000: Satellite earth observation in operational oceanography. *Coastal Eng.,* **41** (1–3), 155–176.

Lin, I.-I., W. Alpers, and W. T. Liu, 2003: First evidence for the detection of natural surface films by the QuikSCAT scatterometer. *Geophys. Res. Lett.,* **30**, 1713, doi:10.1029/2003GL017415.

McClain, E. P., and A. E. Strong, 1969: On anomalous dark patches in satellite-viewed sunglint areas. *Mon. Wea. Rev.,* **97,** 875–884.

McPhaden, M. J., and Coauthors, 1998: The Tropical Ocean-Global Atmosphere observing system: A decade of progress. *J. Geophys. Res.,* **103,** 14 169–14 240.

Mitchum, G. T., 2000: An improved calibration of satellite altimetric heights using tide gauge sea levels with adjustment for land motion. *Mar. Geod.,* **23,** 145–166.

Moller, D., P. D. Mourad, and S. J. Frasier, 2000: Field observations of radar backscatter from the ocean surface under low wind speed conditions. *J. Geophys. Res.,* **105,** 24 059–24 069.

Moore, R. K., and C. S. Williams, 1957: Radar terrain return at near-vertical incidence. *Proc. IRE,* **45,** 228–238.

Plant, W. J., D. E. Weissman, W. C. Keller, V. Hessany, K. Hayes, and K. W. Hoppel, 1999: Air/sea momentum transfer and the microwave cross section of the sea. *J. Geophys. Res.,* **104,** 11 173–11 191.

Quartly, G. D., M. A. Srokosz, and A. C. McMillan, 2001: Analyzing altimeter artifacts: Statistical properties of ocean waveforms. *J. Atmos. Oceanic Technol.,* **18,** 2074–2091.

Rodriguez, E., 1988: Altimetry for non-Gaussian oceans: Height biases and estimation of parameters. *J. Geophys. Res.,* **93,** 14 107–14 120.

Shankaranarayanan, K., and M. A. Donelan, 2001: A probabilistic approach to scatterometer model function verification. *J. Geophys. Res.,* **106,** 19 969–19 990.

Vandemark, D., J. Edson, and B. Chapron, 1997: Altimeter estimation of sea surface wind stress for light to moderate winds. *J. Atmos. Oceanic Technol.,* **14,** 716–722.

Wu, J., 1991: Effects of atmospheric stability on ocean ripples: A comparison between optical and microwave measurements. *J. Geophys. Res.,* **96,** 7265–7269.

Zieger, A. R., D. W. Hancock, G. S. Hayne, and C. L. Purdy, 1991: NASA radar altimeter for the TOPEX/POSEIDON project. *Proc. IEEE,* **79,** 810–826.